

Cd concentration effect on structural, optical and electrical properties of $\text{Cu}_2(\text{Cd}_x\text{Zn}_{1-x})\text{SnS}_4$

D. Juárez*, H. E. Castillo García

Instituto de Energías Renovables, Universidad Nacional Autónoma de México, Temixco, Morelos, 62580, México

*) E-mail: djrez@ier.unam.mx



Received 11/9/2018, Accepted 17/12/2018, Accepted 15/1/2019

In this paper we are reporting an in-depth study into the material properties of cadmium incorporated kesterite material $\text{Cu}_2(\text{Cd}_x\text{Zn}_{1-x})\text{SnS}_4$ (CZCTS). Though it was reported in the past that CZCTS can be a candidate solar cell material, little is known about the material characteristics of this compound. In this work, the impact of Cd content on structural, morphological, optical, electrical and opto-electronic properties of CZCTS films is studied by XRD, Raman, EDXS, SEM, UV-Vis, Seebeck effect, photoconductivity, I-T, Kelvin probe, and Hall measurements. It was found that the CZCTS band-gap varies almost linearly with the Cd concentration in CZTS lattice. Photosensitivity, carrier concentration and work function showed a clear tendency with respect to Cd content. The in-depth material characterizations and in particular the electrical and opto-electronic data presented in this paper will help designing opto-electronic devices based on this material.

Keywords: $\text{Cu}_2(\text{Cd}_x\text{Zn}_{1-x})\text{SnS}_4$; Kesterite; Solar materials.

1. INTRODUCTION

$\text{Cu}_2\text{ZnSnS}_4$ (CZTS) semiconductor has been widely studied as a potential absorber material due to its adequate physical properties for solar cell applications as well as the abundance of its constituents. In particular, this semiconductor is described by p-type conductivity, a direct band-gap near to 1.5 eV which is close to the optimal one for single-junction solar cells, and relatively high optical absorption coefficient [1-3]. However, efficiency of CZTS solar cells has been mainly limited by the large open-circuit voltage deficit, which is a result of the cationic (Cu/Zn) disorder resulting from similar ion radius of Cu and Zn, contributing to the formation of Cu_{Zn} antisite defects [4-6]. In order to reduce the density of defects associated to

Cu/Zn disorder for promoting kesterite solar cell efficiency, the partial replacement of Zn atoms by other elements with relatively higher radius is highly recommended. In this sense, Cd is characterized by larger radius than those of Cu and Zn and hence incorporation of Cd into CZTS lattice may reduce the formation of Cu_{Zn} antisite defects which in turn can enhance open-circuit voltage. In fact, an efficiency improvement from 5.3% for reference CZTS device to 9.2% for $\text{Cu}_2\text{Zn}_{0.6}\text{Cd}_{0.4}\text{SnS}_4$ (CZCTS) has been demonstrated [7], supporting the advantages of Cd alloying in CZTS compound. More recently, an efficiency of 11.5% with reduced open-circuit voltage deficit was reported for Cd alloyed CZTS solar cells [8]. It was found that the introduction of Cd can reduce the band-tailing issue while improving the microstructure, minority carrier lifetime and electrical properties of CZTS absorber [8]. Another important feature associated to Cd alloying is the band-gap lowering from 1.55 to 1.09 eV in $\text{Cu}_2(\text{Cd}_x\text{Zn}_{1-x})\text{SnS}_4$ when x is changed from 0 to 1 [8,9]. As a result, unlike most reported works on reaching ideal band-gap values by changing S/Se compositional ratio in CZTSSe [10], the Cd alloying to obtain $\text{Cu}_2(\text{Cd}_x\text{Zn}_{1-x})\text{SnS}_4$ compound could favor not only the reduction of Cu/Zn disorder defects but also achieving an optimal band-gap. As an interesting point, a band-gap grading could be also achieved for CZCTS compound by controlling Cd/(Zn+Cd) compositional ratio which could be an alternative choice to band-gap grading based on S/Se compositional ratio. Furthermore, the use of CdS with low enthalpy of formation as the Cd source can enlarge the single-phase region reducing the formation of secondary phases which is also an important aspect in this

technology [7]. Therefore, $\text{Cu}_2(\text{Cd}_x\text{Zn}_{1-x})\text{SnS}_4$ compound is presented as a potential candidate for promoting current kesterite solar cell technology. However, in comparison to CZTSSe compound, fewer studies are found on the physical properties of Cd incorporated CZCTS. In particular lacking information on the role that Cd element is playing on electrical properties of CZCTS. This study could help for a better understanding of mechanisms behind Cd alloying processes contributing to a further promotion of CZCTS solar cell efficiency.

So far, only few studies where CZCTS compound was processed through sol-gel [7, 11, 12], spin-coating [13-16], electrospinning [17], and a hybrid approach where CZTS precursors were deposited by sputtering followed by depositing CdS by chemical bath deposition. In the latter case a post-deposition thermal annealing of the stack in sulfur atmosphere was performed [8]. In this paper, we are discussing the impact of Cd/(Zn+Cd) compositional ratios

on the physical properties of CZCTS thin film. The impact of Cd concentrations on structural, morphological, optical and electrical properties of CZCTS thin films are studied in detail.

2. EXPERIMENTAL DETAILS

The CZCTS thin films were developed on corning glass substrates in order to facilitate various studies. The first layer CdS with different thicknesses were deposited by chemical bath deposition at 80 °C from a bath containing $\text{Cd}(\text{NO}_3)_2$ (0.1 M), $\text{Na}_3\text{C}_6\text{H}_5\text{O}_7$ (1 M), NH_4OH (1 M) and $\text{CH}_4\text{N}_2\text{S}$ (1 M) in deionized water. The thickness of CdS layers was decided by the time duration substrate was immersed in the bath. The second step was the sequential deposition of binary sulfides in the following order: CuS/SnS/ZnS on top of CdS. Finally, the thin film stack was submitted to thermal annealing under N_2 and S atmosphere. The CuS and SnS thicknesses were set at 600 and 950 nm respectively, while the thickness of ZnS was reduced from 120 nm to 80 nm in steps of 10 nm in order to match with the CdS thickness increase in the range of 60 – 140 nm with a step of about 20 nm. This particular film thicknesses were selected on the basis of different experiments, in order to obtain CZCTS films with different Cd/(Zn+Cd) compositional ratios. The corresponding samples were labeled as CZCTS1 (ZnS: 120 nm, CdS: 60 nm), CZCTS2 (ZnS: 110 nm, CdS: 80 nm), CZCTS3 (ZnS: 100 nm, CdS: 100 nm), CZCTS4 (ZnS: 90 nm, CdS: 120 nm) and CZCTS5 (ZnS: 80 nm, CdS: 140 nm). This combinations provided CZCTS films with Cu/(Zn+Cd+Sn) and (Zn+Cd)/Sn compositional ratios close to the optimum values required for kesterite solar cells (Cu-poor and Zn-rich samples) [18]. Furthermore, in this study, Cd/(Zn+Cd) compositional ratio in the range of 0.3-0.7 was chosen, which is close to the optimal value reported for CZCTS solar cells [8]. The thermal annealing process was carried out under nitrogen and 15 mg of sulfur in a sealed oven which was evacuated and purged with nitrogen to minimize the oxygen level. Samples were first annealed at 350 °C during 30 min under a chamber pressure of 600 mTorr to allow the diffusion of elements and in turn the formation of CZCTS compound followed by a second annealing step at 550 °C for 20 min under a pressure of 1Torr to promote recrystallization. A ramp rate was 20 °C/min in both cases and after completing the annealing the oven is left to cool naturally to room temperature (approximately 2-3 h).

The structural properties of CZCTS thin films were studied by X-ray diffraction (XRD) patterns with a Rigaku X-ray diffractometer operating at 40 kV and 40 mA by using Cu-K α radiation ($\lambda = 0.15405$ nm). XRD patterns of the films were recorded by scanning 2θ in the range 10–80°, with a grazing incidence angle of 1°. The elemental composition of the thin films was determined by energy dispersive X-ray spectroscopy (EDXS) using a SEM, model Hitachi SU I510. The Raman measurements were performed in a back-scattering geometry. The set-up consists of a confocal microscope with 60x objective, a diode-pumped solid state (DPSS) laser at a wavelength of 515 nm, a notch filter for removal of scattered laser light, and a Horiba iHR550 spectrometer with a Peltier-cooled CCD detector. The calibration of the spectrometer was verified before each measurement by acquiring Raman Spectra of a standard silicon wafer. A field emission scanning electron microscope (Hitachi FE-SEM S-5500) was employed for surface and cross sectional morphology of CZCTS films. For CZCTS band-gap calculation, transmittance and reflectance data were recorded by a Shimadzu 3101 UV–Vis spectrophotometer. Thermoelectric measurements were performed in a home-made Seebeck system. The electrical properties such as carrier concentration, mobility, resistivity, and the conductivity type of the films were measured by Hall Effect at room temperature applying a magnetic field of 0.36 T using a HS-3000 Hall system. The photoresponse measurements were performed under constant DC bias of 1 V and recorded each second in the following sequence: 5 s in dark, 5 s under illumination (850 W/m²), and finally 5 s in dark. The electrical contacts were taken from two carbon electrodes painted

over the film in a co-planar configuration. The setup consists of a Keithley 230 voltage source and a Keithley 619 electrometer. Current-temperature (I-T) measurements were performed in order to study activation energies in the temperature range 25-280 K. Furthermore, work function measurements were performed with an Ambient Kelvin Probe KP050, KP Technology using an Au probe of known work function (-5.021 eV). All measurements were carried out on two batches of films processed at identical conditions and the characterization results were found to be reproducible.

3. RESULTS AND DISCUSSION

3.1 Structure and composition

Elemental compositions as well as Cu/(Zn+Cd+Sn), (Zn+Cd)/Sn and Cd/(Zn+Cd) ratios of CZCTS samples calculated from EDXS are summarized in Table 1. All samples showed

Cu/(Zn+Cd+Sn) and (Zn+Cd)/Sn compositional ratios near to the ones identified as optimal for solar cell applications [18]. Furthermore, sulfur concentrations about 50% were obtained. Partial replacement of Zn atoms with Cd is evident and systematically increasing from CZCTS1 to CZCTS5 as expected. Results on XRD of CZCTS samples grown under different Cd/(Zn+Cd) compositional ratios are presented in Fig. 1. The highest contributions to diffraction are observed from planes (112), (200), (220), (312) and (332) which are ascribed to $\text{Cu}_2\text{ZnCdSnS}_4$ compound with tetragonal structure as per PDF: 26-0575 and PDF: 29-0537 for $\text{Cu}_2\text{ZnSnS}_4$ and $\text{Cu}_2\text{CdSnS}_4$ (CCTS) respectively. These results are in good agreement with previously published works [7, 13, 19, 20]. A small contribution from planes (110) and (008) attributed to the $\text{Cu}_2\text{ZnCdSnS}_4$ compound is also illustrated. The behavior of diffraction plane (112) as a function of Cd/(Zn+Cd) compositional ratio is presented in Fig. 2. A peak shift towards lower angles with increase in Cd/(Zn+Cd) compositional ratio is clearly observed, which is a result of partial replacement of Zn atoms by Cd as previously reported [7, 13, 19]. This behavior is in good correspondence with results presented in Table 1. From a previous theoretical work, it has been demonstrated that substitution energies of Cd atoms at Cu, Sn and Zn sites in CZTS lattice are $E_{\text{sub}}(\text{Cd}_{\text{Cu}}) = 0.69\text{eV}$, $E_{\text{sub}}(\text{Cd}_{\text{Sn}}) = 1.07\text{ eV}$ and $E_{\text{sub}}(\text{Cd}_{\text{Zn}}) = 0.53\text{ eV}$ [20]. Therefore, Cd substitution at Zn sites is the most likely isoelectronic substitution. On the other hand, the presence of Cu vacancies under the present conditions (Cu-poor and Zn-rich samples) can also favor Cd substitution at Cu sites forming charge-neutral ($\text{Cd}_{\text{Cu}} + \text{V}_{\text{Cu}}$) pairs [20]. Crystallite size and strain values were estimated from Williamson-Hall method and results are presented in Table 1. Small variations of crystallite sizes in the range of 33.8 – 53.1 nm were obtained. In particular, the highest crystallite sizes are obtained for samples CZCTS1 and CZCTS2 which present Cd/(Zn+Cd) compositional ratios near to the optimal values suggested for solar cells [8]. As an interesting result, in a previous work improvements in surface morphology and crystal growth were observed at the optimal Cd/(Zn+Cd) compositional ratio [15]. Consequently, CZCTS1 and CZCTS2 are identified as more adequate for solar cell applications. On the other hand, a slight but systematic increase in strain value is also obtained from CZCTS1 to CZCTS5 which is likely to be related to the partial substitution of Zn atoms by Cd atoms. In this sense, CZCTS1 and CZCTS2 samples present the lowest strain values and in turn the lowest structural distortion. As an interesting feature, an identical trend was observed for crystallite size (Table 1) and the intensity of reflection from plane (112) with increasing Cd/(Zn+Cd) compositional ratio (Fig. 1). The

observed decrease in (112) peak intensity for samples CZCTS1 to CZCTS3 coincides with the decrease in crystallite size. For Cd/(Zn+Cd) compositional ratios higher than 0.54, a slight increase of both crystallite size and (112) peak intensity is observed. The CZCTS1 sample displayed the highest (112) peak intensity along with the largest crystallite size supporting it as the adequate material from the structural point of view.

Table 1 Elemental compositions, Cu/(Zn+Cd+Sn), (Zn+Cd)/Sn and Cd/(Zn+Cd) ratios, crystallite size and strain obtained from Williamson-Hall analysis for CZCTS samples.

sample	Cu (%)	Zn (%)	Cd (%)	Sn (%)	S (%)	Cu/ (Zn+Cd+Sn)	(Zn+Cd)/ Sn	Cd/ (Zn+Cd)	Crystallite Size (nm)	strain
CZCTS1	123.54	9.53	4.49	11.28	51.16	0.93	1.24	0.32	53.1	0.00046
CZCTS2	223.56	9.23	5.19	11.68	50.34	0.90	1.23	0.36	49.5	0.00103
CZCTS3	322.97	6.88	8.07	12.46	49.62	0.84	1.20	0.54	33.8	0.00112
CZCTS4	423.52	5.60	8.75	11.56	50.57	0.91	1.24	0.61	42.5	0.00126
CZCTS5	523.37	4.83	9.80	11.84	50.16	0.88	1.24	0.67	46.4	0.00198

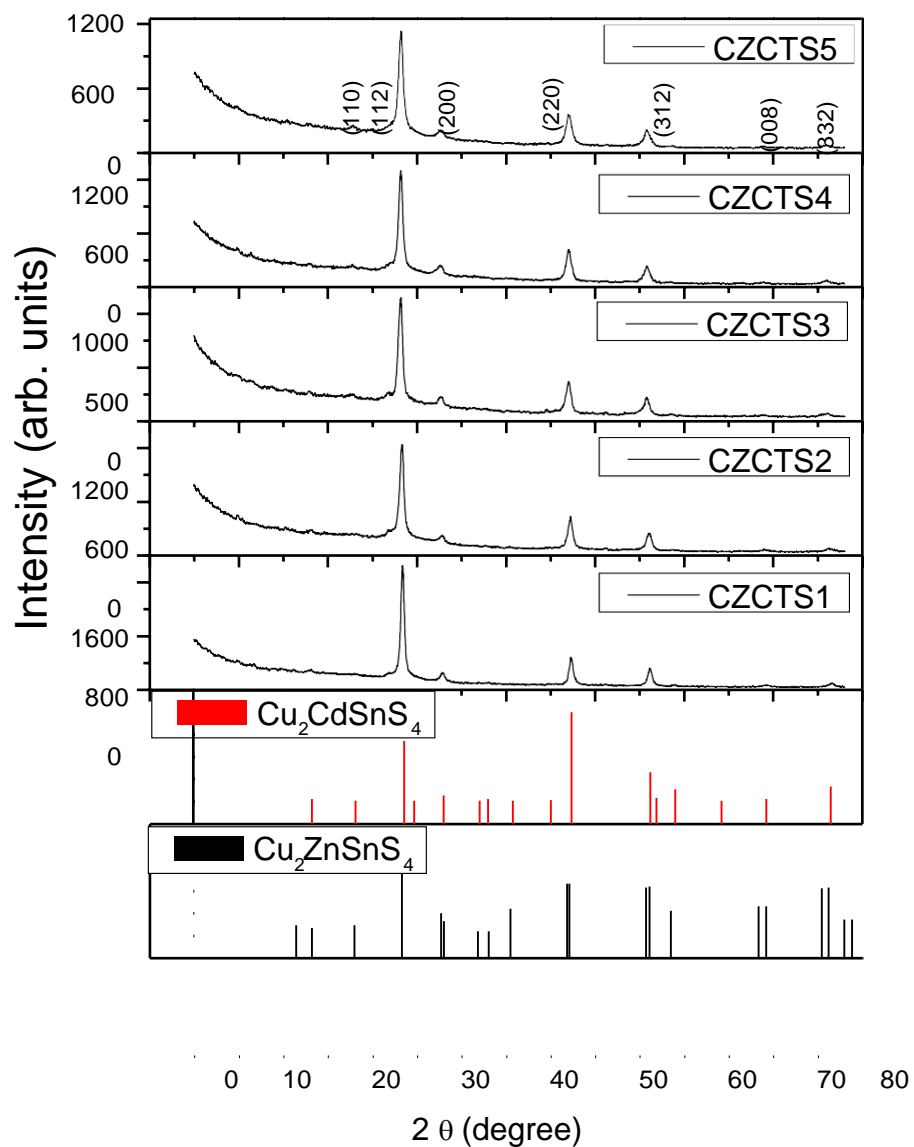


Figure 1 XRD patterns of CZCTS thin films processed under different Cd/(Zn+Cd) compositional ratio.

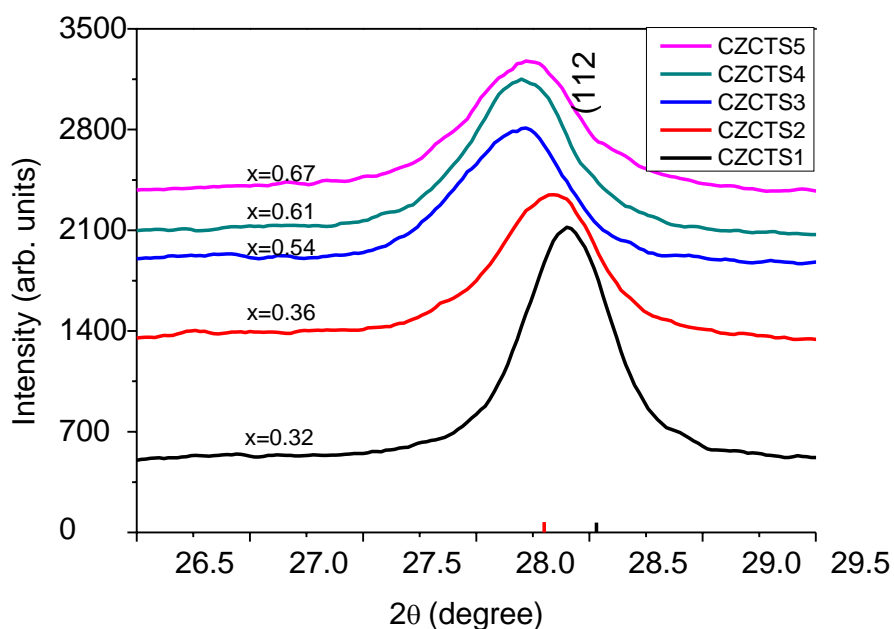


Figure 2 Shift of the (112) XRD peak in CZCTS thin films as a function of Cd/(Zn+Cd) compositional ratio.

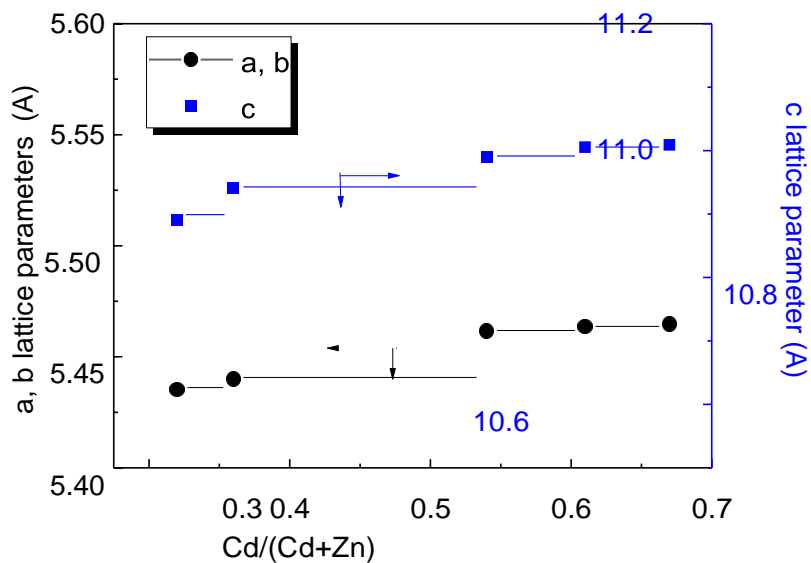


Figure 3 Lattice parameters of tetragonal CZCTS thin films as functions of Cd/(Zn+Cd) compositional ratio.

Lattice parameters from tetragonal structure were calculated from XRD data and results are presented in Fig. 3. The calculated a and c lattice values are in good correspondence with those reported for $\text{Cu}_2\text{ZnCdSnS}_4$ compound with tetragonal structure as previously published [7, 13, 19]. In particular, an increase of both a and c parameters with increasing $\text{Cd}/(\text{Cd}+\text{Zn})$ ratio is observed which is a result of partial replacement of Zn atoms with higher radii Cd atoms as reported elsewhere [7, 13, 19]. From lattice parameters, tetragonal distortion parameter ($c/2a$) was calculated which allows identifying the prominent phase, kesterite or stannite in samples. Distortion parameter lower or equal to 1 has been identified as kesterite while values higher than 1 indicates the stannite structure [21]. In our case, all samples were characterized by kesterite structure. In a recent work, it was observed that for $\text{Cd}/(\text{Zn}+\text{Cd})$ compositional ratio higher than 0.7, the (220) plane starts to split into (220) and (204) planes, confirming the transition from kesterite to stannite [13]. Therefore, from our XRD results, the formation of kesterite structure is confirmed as no split is observed under $\text{Cd}/(\text{Zn}+\text{Cd})$ compositional ratios in the range of 0.3–0.7. The kesterite structure in CZCTS compound was also found in references [7] and [15] for $\text{Cd}/(\text{Zn}+\text{Cd})$ compositional ratios lower than 0.7. Finally, it is worth mentioning that the presence of possible binary or ternary secondary phases was not detected in the XRD data.

In order to acquire information on the preferential orientation of the crystallites, the texture coefficient ($_{(hkl)}$) was calculated using the relation:

$$TC_{(hkl)} = \frac{I_{(hkl)}/I_{o(hkl)}}{N^{-1} \sum_N I_{(hkl)}/I_{o(hkl)}} \quad (2)$$

where $I_{o(hkl)}$ and $I_{(hkl)}$ are respectively the relative intensities of the plane (hkl) obtained from the powder sample (JCPDS data) and that measured on the sample under study, and N is the number of diffraction peaks. Results on the texture coefficient as a function of Cd incorporation for planes (112), (200), (220) and (312) are presented in Fig. 4. When $_{(hkl)} \leq 1$, the crystallites are randomly oriented and when it is greater than unity crystallites has a preferred growth along that particular plane. From Fig. 4, it is clear that the samples present a

preferred orientation along (112) plane which is more significant when 54% of Zn atoms are replaced by Cd atoms. A preferential orientation along (112) plane has been previously reported for kesterite family [1].

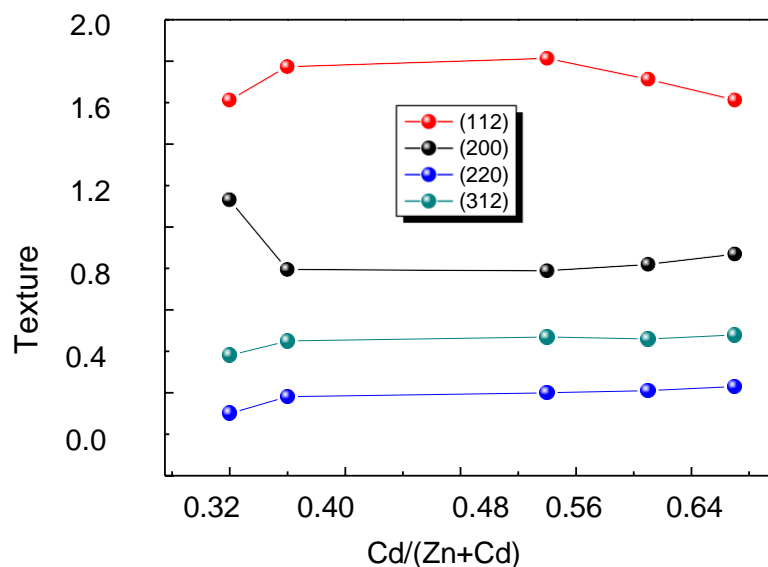
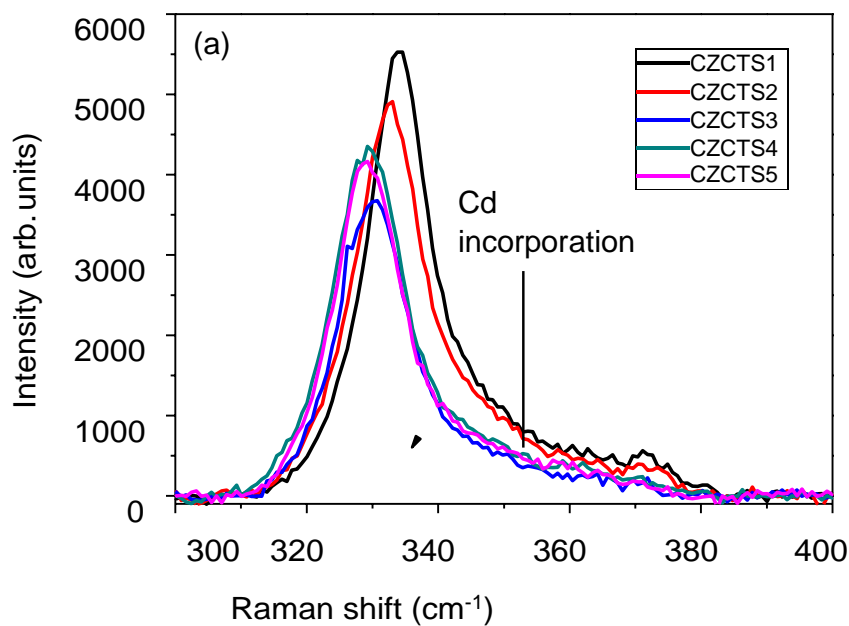


Figure 4 Texture coefficient for (112), (200), (220) and (312) planes of CZCTS thin films as a function of Cd/(Zn+Cd) compositional ratio.

Raman measurements were carried out in order to corroborate the CZCTS formation. Results on CZCTS thin films are presented in Figure 5. A1 mode positions at 338 and 326 cm^{-1} have been previously reported for CZTS and CCTS compounds, respectively [2, 22], which are associated to vibrational motion involving sulfur atom with Zn and Cd, respectively, in these compounds [13]. In this sense, the A1 mode of CZCTS compound with peak positions between those associated to CZTS and CCTS as a function of Cd incorporation is detected from Fig. 5, in agreement with previous reports [13]. Particularly, a shift towards lower wavelength values with Cd incorporation is clearly observed from Fig. 5b. For Cd/(Zn+Cd) compositional ratios lower than 0.6, a nearly linear shift of main A1 mode is observed while subsequent increase in Cd concentration did not affect the frequency of main A1 mode. This result coincides with a previous report [19]. Cd atoms are characterized by higher mass than Zn, hence the replacement of Zn with Cd can result in frequency shift towards lower values. This

result is in good agreement with the results on composition and stress observed in XRD analysis. The slight increase of FWHM of main A1 peak with Cd incorporation can be interpreted as due to perturbations in crystalline lattice which coincides with XRD results and the literature reports on FWHM values of CZCTS as a function of Cd incorporation [13]. Further, a decrease in Raman intensity can be observed as a result of Cd incorporation, indicating a degradation in crystalline quality. The asymmetry of main A1 mode towards the higher wavenumber side could be attributed to a contribution from CZTS, which is more evident for CZCTS samples with least amount of Cd. It should be noted that no evidence of secondary phases was detected in Raman spectra.



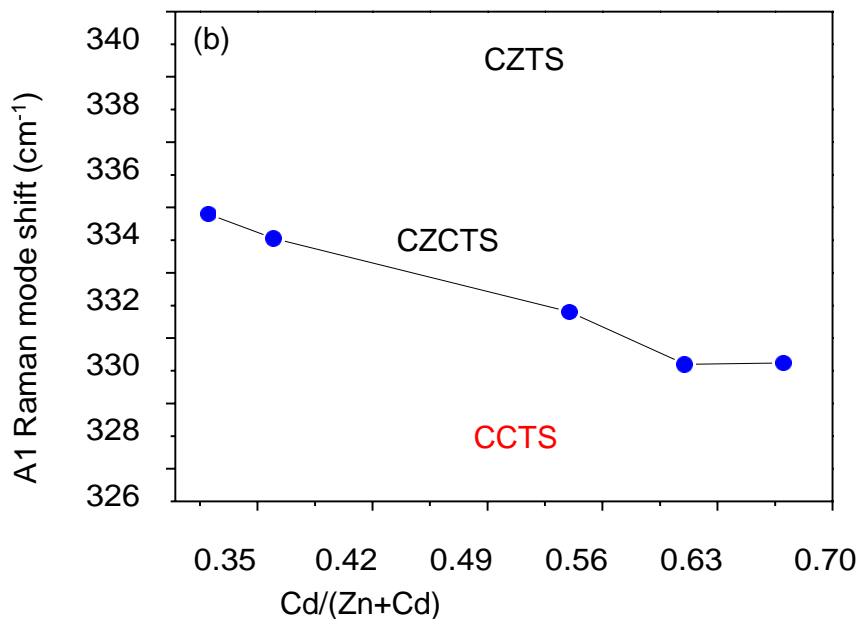


Figure 5 (a) Raman spectra of CZCTS thin films processed under different Cd concentrations, and (b) A1 peak position as a function of Cd/(Zn+Cd) compositional ratio.

3.2 Morphological properties

SEM micrographs of CZCTS surface and cross-section are presented in Fig. 6. Different surface morphologies depending on Cd content was observed. For the lowest Cd concentration (CZCTS1), homogenous, well defined large grains are observed. As the Cd content increased the grains got smaller and at higher Cd concentrations the smaller grains start to coalesce forming big clusters. The thickness of the samples as seen in the cross- section is in the range of 1.5 μm , and in general very compact and free of voids. Better crystallization is observed for samples CZCTS1 and CZCTS2, which are characterized by the lowest Cd concentrations; this result is expected based on the XRD and Raman results discussed above. The Cd/(Cd+Zn) compositional ratio of these samples are in the range 0.32 to 0.36 (Table 1), which is in the range of values reported in literature for device quality CZCTS [15].

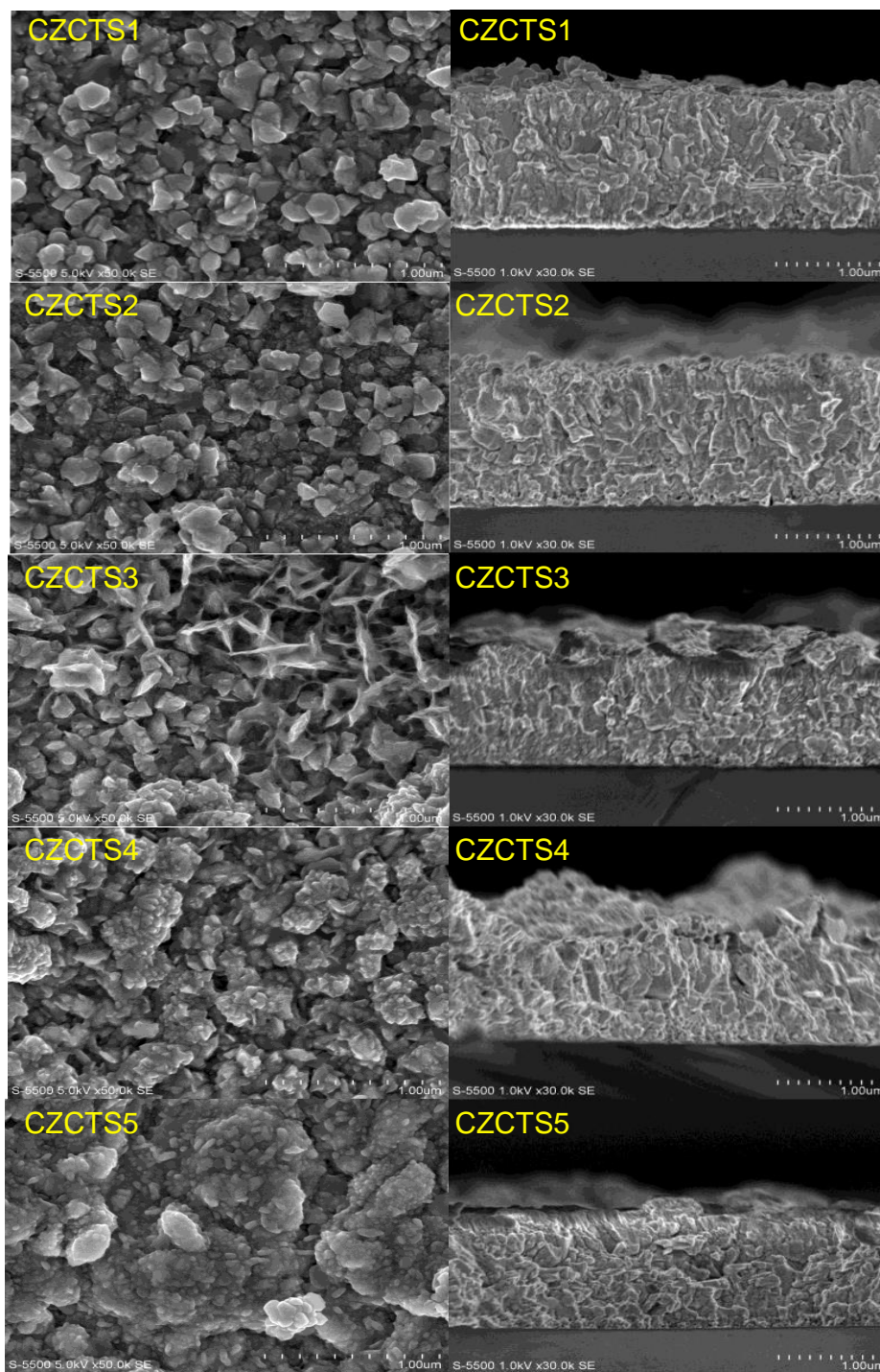


Figure 6 Surface and cross-section micrographs of CZCTS thin films processed with different Cd concentrations.

3.3 Optical properties

The impact of Cd content on CZCTS band-gap value was studied by recording the transmittance and reflectance of the films. Under multiple reflections condition, the absorption coefficient (α) is defined as:

$$\alpha = \frac{1}{d} \ln \left[\frac{(1-R^2) + \sqrt{4R^2T^2}}{2T} \right] \quad (3)$$

where R and T the reflectance and transmittance as a functions of wavelength, and d is the CZCTS film thickness. From absorption coefficient data, CZCTS band-gap (E_g) is calculated for allowed direct transitions from the linear plot $(\alpha h\nu)^2$ vs. $h\nu$, where $h\nu$ is the photon energy. Band-gap values in the range of 1.17 – 1.25 eV are estimated (Fig. 7). The inset of Fig. 7 is the variation of E_g with Cd/(Zn+Cd), showing a nearly linear dependence. The CZTS compound has been often described by a band-gap near to 1.5 eV [1] while band-gap values as low as 1.14 eV have been reported for CCTS thin films [22]. Therefore, the introduction of Cd into CZTS lattice can help to tailor the band-gap. A fitting function was determined for the E_g vs. Cd/(Zn+Cd) plot giving a bowing parameter $b = 0.05$, which accounts for the high linearity [13]. So far, the cause of band-gap lowering in CZCTS thin films with Cd incorporation is not well understood. The conduction band minimum (CBM) is mainly affected by the antibonding component of the s-s and s-p hybridization between the Sn^{4+} and S^{2-} , while the valence band maximum (VBM) is mainly controlled by the antibonding component of the p-d hybridization between S^{2-} and Cu^+ [23]. Consequently, the partial substitution of Zn^{2+} with Cd^{2+} should not modify the band-gap value. In order to provide a possible explanation, Su et. al. considered that band-gap reduction with Cd incorporation could be a result of the expansion of CZTS unit cell volume that would weaken the antibonding component of the s-s and s-p hybridization between the Sn^{4+} and S^{2-} leading to a reduction of CBM [7].

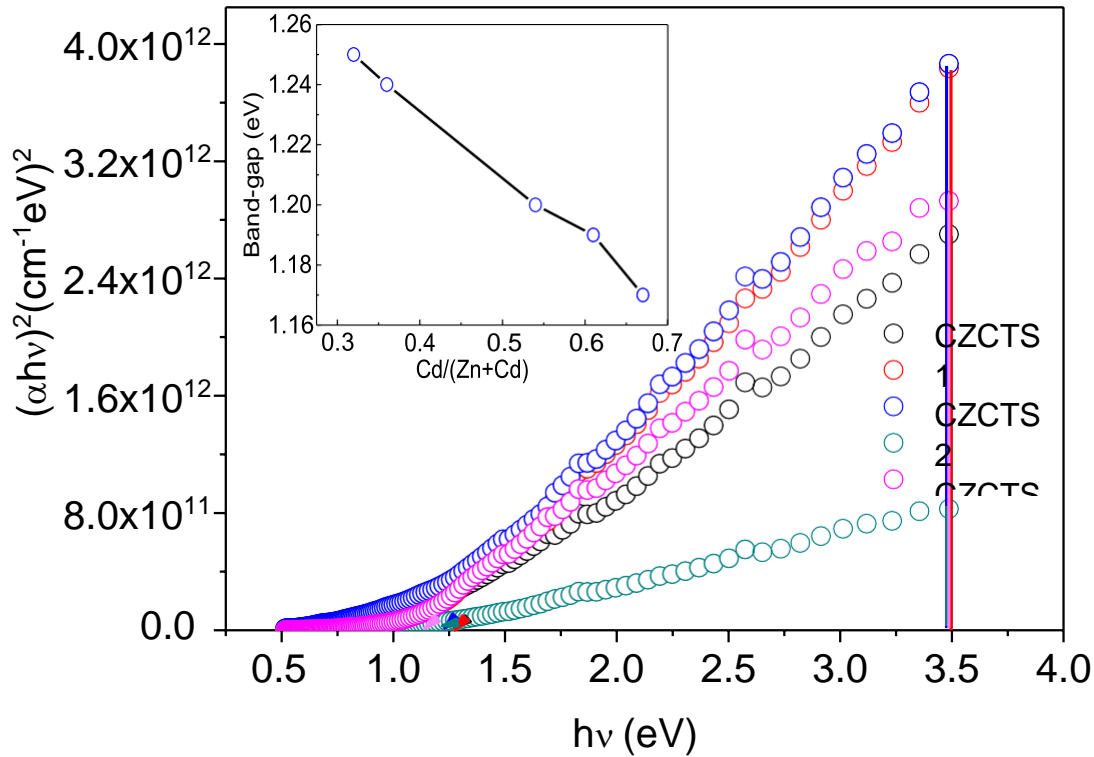


Figure 7 Band-gap determination for CZCTS thin films processed with different amounts of Cd. Inset shows the variation of band gap with increase of Cd content in the film.

Information on defect formation can be obtained by Urbach tail model. According to Urbach model, the semilog plot of absorption vs. photon energy should give a linear fit where the slope yields to the inverse of Urbach energy. A lower Urbach energy accounts to a better crystallized material with less defects [8, 24]. Urbach energy for each sample was calculated as presented in the inset of Fig. 8 and its dependence on Cd incorporation is plotted in Fig. 8. As an important feature, Urbach energy is higher for films with more Cd, which implies a higher lattice disorder with Cd incorporation, this observation is in agreement with XRD, Raman and SEM results.

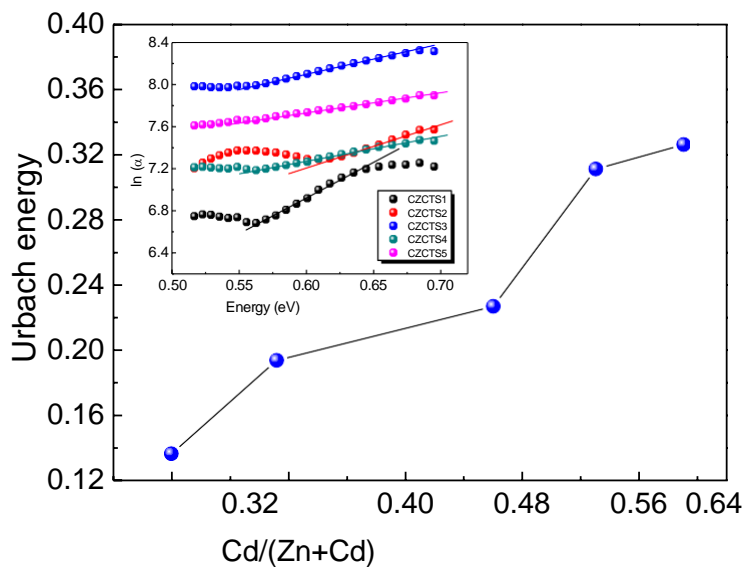


Figure 8 Urbach energy for CZCTS thin films processed with different amounts of Cd. Inset: plot of $\ln(\alpha)$ vs. energy ($h\nu$) for estimating Urbach energy.

3.4 Electrical properties

The impact of Cd incorporation on CZCTS electrical properties is a topic studied little in literature. Seebeck measurements were performed to acquire information on electrical properties of CZCTS thin films. As far as we know, there is no report on Seebeck measurements in CZCTS compound. Results on Seebeck measurements are presented in Fig. 9. The positive slope of the thermoelectric power demonstrate p-type conductivity for all samples. Thermoelectric power values in the range of 350 – 513 $\mu\text{V}/\text{K}$ were calculated for CZCTS samples. A tendency to lower the thermoelectric power is observed with the Cd incorporation into the lattice. This behavior could be related to the decrease in hole carrier concentrations with Cd incorporation. That is, higher the thermoelectric power higher is the voltage created by diffused holes as a result of temperature difference.

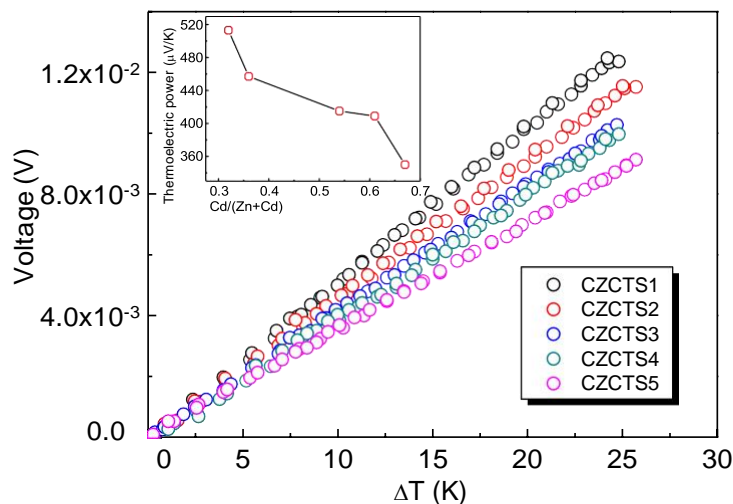


Figure 9 Seebeck measurements for CZCTS thin films processed under different Cd concentrations. Inset: Thermoelectric power as a function of Cd/(Zn+Cd) compositional ratio

In order to study the potential application of these samples in solar cells, photoconductivity measurements were performed and the results are presented in Fig. 10(a). A decrease in photoconductivity with Cd incorporation is clearly observed. In particular, CZCTS1 displayed a response close to the ideal case (fast rise and fast decay) which accounts to a better crystalline quality. In fact, from XRD, Raman and SEM characterizations, it has been observed that the best crystallinity is obtained for CZCTS1 sample which supports the photoconductivity data. When Cd is incorporated, a slow rise and decay for the photoresponse is observed, indicating the action of charge traps. Also a tendency to increase the resistivity with Cd incorporation is clearly observed. Despite CZCTS4 and CZCTS5 are resulted as the most resistive samples, their photoresponse values were the lowest ones, which is a result of a higher defect formation contributing to carrier losses. From Fig. 10(a), information on photosensitivity as a function of Cd/(Cd+Zn) compositional ratio can be acquired and the results are summarized in Fig. 10(b). A clear drop of photosensitivity with Cd incorporation into the lattice is illustrated. In this sense, samples with Cd/(Cd+Zn) compositional ratios between 0.3 and 0.4 are better candidates for solar cell applications.

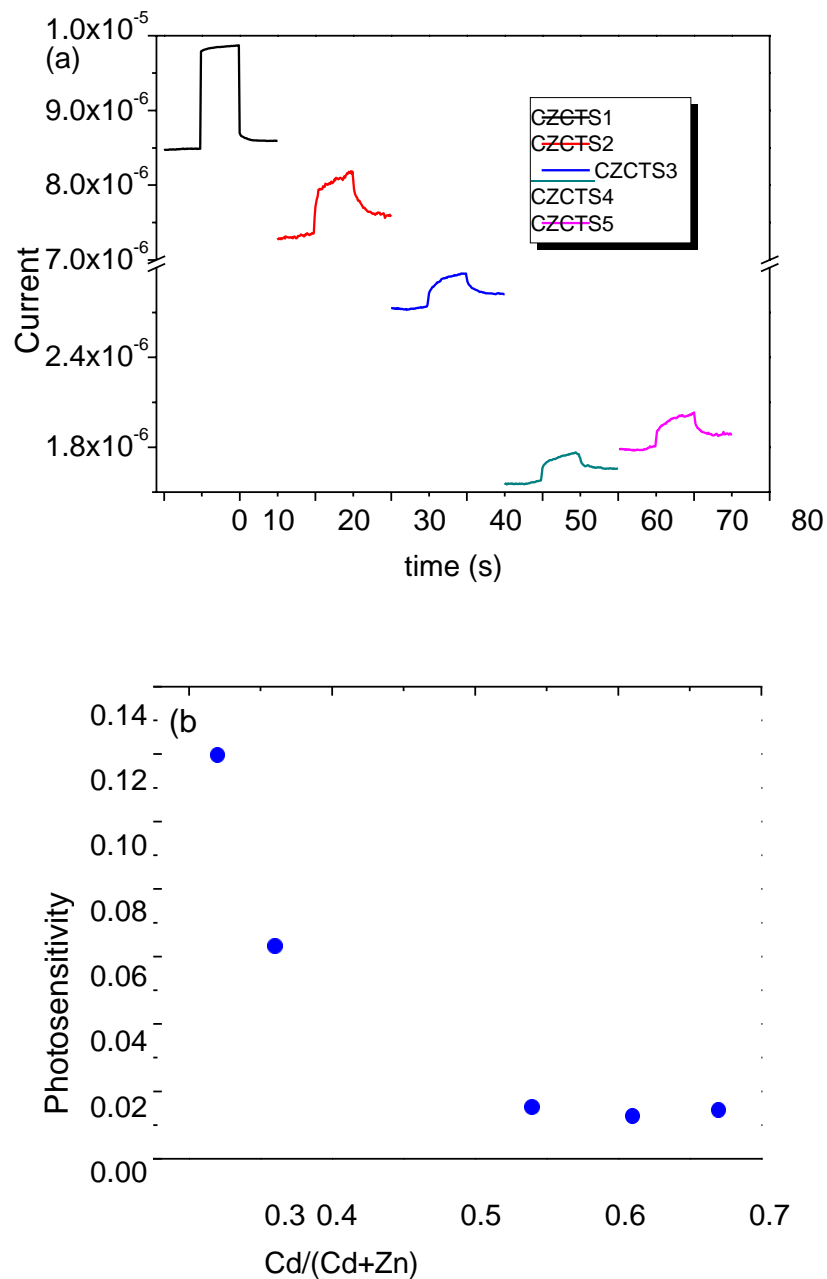


Figure 10 (a)- Photoconductivity measurements for CZCTS thin films processed under different Cd concentrations, and (b)- photosensitivity dependence on Cd/(Zn+Cd) compositional ratio.

Hall Effect measurements were performed to attain information on electrical properties of CZCTS samples. All the samples displayed p-type conductivity confirming results obtained by Seebeck effect measurements. Results on mobility.

hole carrier concentration and resistivity as a functions of Cd/(Cd+Zn) compositional ratios are presented in Fig. 11. Increase in resistivity with Cd incorporation until a Cd/(Cd+Zn) compositional ratio of 0.61 (CZCTS4 sample) is obtained while no meaningful trend was found for mobility values. The increase of CZCTS resistivity with Cd incorporation could be a result of the reduction of hole carrier concentration as presented in Fig. 11 corroborating thereby results obtained by Seebeck measurements where a reduction of thermoelectric power was reported. The resistivity trend observed from Hall measurements is in good agreement with resistivity trend obtained from photoconductivity measurements. For CZTS compound, it has been observed that Cu at Zn sites enables the formation of acceptor-like defects contributing to p- type conductivity of this compound [24] which is a result of similar radius of Cu and Zn atoms. In this sense, the partial replacement of Zn atoms by Cd would avoid the formation of Cu_{Zn} antisites reducing acceptor carrier concentration and in turn resistivity of samples as observed from our results. In fact, a decrease in acceptor concentration with Cd incorporation was previously observed [8]. Values obtained from hole carrier concentration and hole mobility are in correspondence with values reported in reference [11] for CZCTS compound.

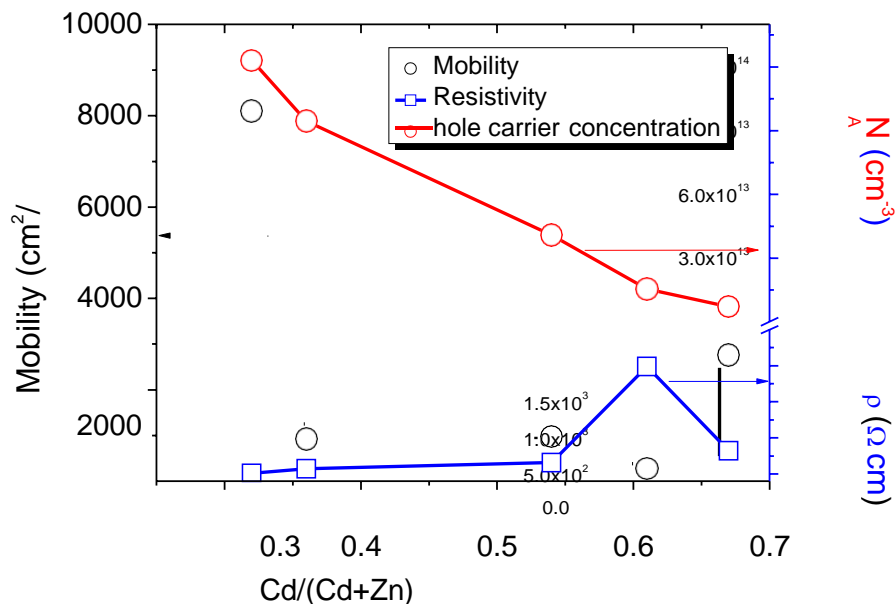


Figure 11 Mobility, hole carrier concentration and resistivity found by Hall measurements for CZCTS thin films with different Cd concentrations.

I-T measurements were performed to acquire more information on the impact of Cd concentration on electrical properties of the kesterite film. From the semilog plot of current vs $1/kT$ (where k is the Boltzmann constant and T the temperature), activation energy values can be estimated as shown in the inset of Fig. 12. The tendency of activation energy to increase with Cd content in film is demonstrated in Fig. 12. The activation energy provides an indication about shallow/deep levels formed within the band-gap which could be a result of bulk and/or grain boundary defects. In this sense, when the substitution of Zn by Cd is less than 40%, shallow defects which are likely to be acceptors are formed, however, for higher Cd incorporation deeper levels are formed which could be acting as recombination centers reducing the photocurrent response as demonstrated in Fig. 10a & b. This is also supported by the observation in Fig. 11 that the hole density is lower for films with higher Cd content. This could be a result of the partial replacement of Zn atoms by Cd avoiding the formation of Cu_{Zn} antisites reducing thereby acceptor carrier concentration as mentioned before.

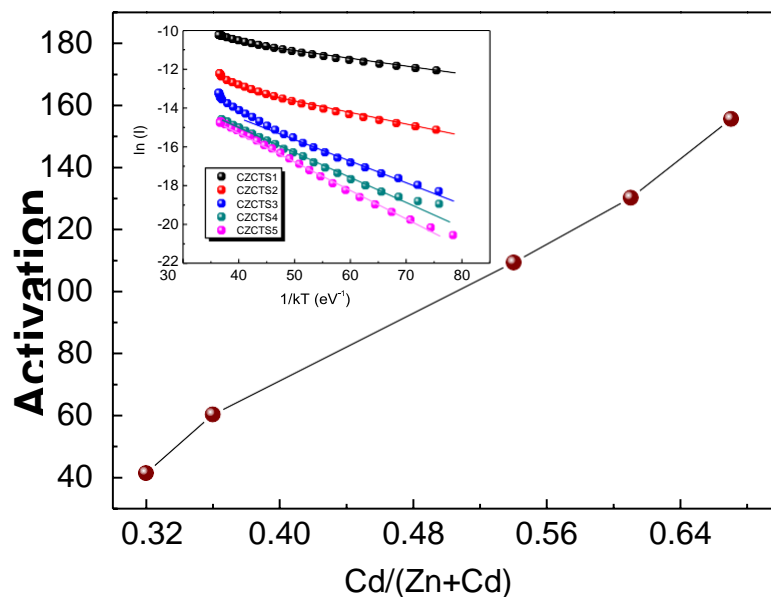


Figure 12 Relation between activation energy and Cd content in film. Inset: Plot of $\ln(I)$ vs. $1/kT$ for activation energy calculation.

Finally, Kelvin-probe measurements were performed to estimate work function of the films. Bearing in mind the well-known mathematical relationship between Fermi energy and carrier concentration from semiconductor physics for doped samples, information on Fermi energy can be obtained once carrier concentration is measured from Hall effect. The electron affinity can be also estimated once the work function and Fermi energy are known. Results on Fermi energy, work function and electron affinity for CZCTS samples as a function of Cd content are presented in Fig. 13. Though the changes are small, a clear tendency is observed for Fermi energy, work function, and electron affinity with respect to the Cd content in the film. The increase in Fermi energy coincides with the tendency to lower hole density as seen in Fig. 11.

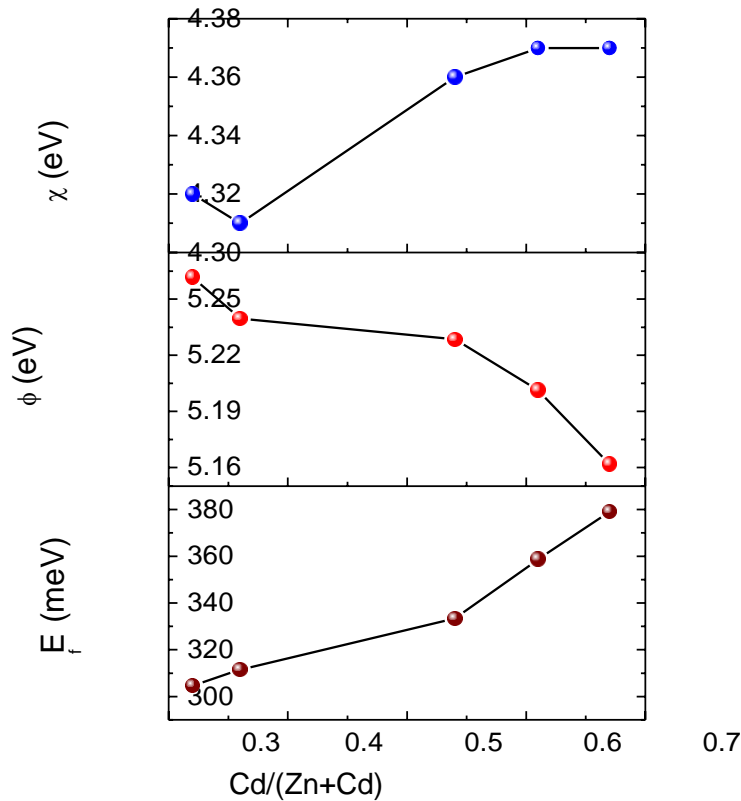


Figure 13 Fermi energy (bottom), work function (middle), and electron affinity (top) as a function of Cd content in films.

4. CONCLUSIONS

Polycrystalline and phase-pure thin films of $\text{Cu}_2(\text{Cd}_x\text{Zn}_{1-x})\text{SnS}_4$ with kesterite structure were developed by post-annealing of a binary sulfide stack $\text{CdS}/\text{CuS}/\text{SnS}/\text{ZnS}$. The $\text{Cd}/(\text{Zn}+\text{Cd})$ compositional ratio of the obtained films were in the range 0.3-0.6. It was observed that the $\text{Cu}_2(\text{Cd}_x\text{Zn}_{1-x})\text{SnS}_4$ band-gap can be tailored with a nearly linear dependence on the amount of Cd incorporated into CZTS lattice. The electrical and opto-electronic parameters of the CZCTS films as a function of Cd content in the film is studied and reported.

Acknowledgments

M. Courel thanks postdoctoral fellowship from DGAPA-UNAM during the experimental development of this work. This work was partially supported by the projects CeMIE-Sol-207450/P28, and PAPIIT- IN102718 and PAPIIT- IN104518. Authors thank Maria Luisa Ramón for the XRD measurements, Rogelio Moran Elvira for taking SEM images and Dr. Oscar Jaramillo for Kelvin probe measurements.

References

- [1] M. Courel, J. A. Andrade-Arvizu, A. Guillén-Cervantes, M. M. Nicolás-Marín, F. A. Pulgarín-Agudelo, O. Vigil-Galán. Optimization of physical properties of spray-deposited $\text{Cu}_2\text{ZnSnS}_4$ thin films for solar cell applications. *Materials & Design* 114 (2017) 515
- [2] T.G. Sánchez, X. Mathew, N.R. Mathews. Obtaining phase-pure CZTS thin films by annealing vacuum evaporated $\text{CuS}/\text{SnS}/\text{ZnS}$ stack. *Journal of Crystal Growth*. 445 (2016) 15
- [3] J. J. Scragg, P. J. Dale, L. M. Peter, G. Zoppi, I. Forbes. New routes to sustainable photovoltaics: evaluation of $\text{Cu}_2\text{ZnSnS}_4$ as an alternative absorber material. *Physica Status Solidi B* 245 (2008) 1772
- [4] S. Bourdais, C. Choné, B. Delatouche, A. Jacob, G. Larramona, C. Moisan, A. Lafond, F. Donatini, G. Rey, S. Siebentritt, A. Walsh, G. Dennler. Is the Cu/Zn Disorder the Main Culprit for the Voltage Deficit in Kesterite Solar Cells?. *Adv. Energy Mater.* 6 (2016) 1502276
- [1] G. Krammer, C. Huber, T. Schnabel, C. Zimmermann, M. Lang, E. Ahlswede, H. Kalt, M. Hetterich. Order-disorder related band gap changes in $\text{Cu}_2\text{ZnSn}(\text{S},\text{Se})_4$: impact on solar cell performance, in: *Proc. 42nd IEEE Photovoltaic Specialist Conference (PVSC)*, (2015)
- [2] K. Timmo, M. Kauk-Kuusik, M. Pilvet, T. Raadik, M. Altosaar, M. Danilson, M. Grossberg, J. Raudoja, K. Ernits. Influence of order-disorder in $\text{Cu}_2\text{ZnSnS}_4$ powders of monograin layer solar cells. *Thin Solid Films* 633 (2017) 122
- [3] Z. Su, J. M. R. Tan, X. Li, X. Zeng, S. K. Batabyal, L. H. Wong. Cation Substitution of Solution-Processed $\text{Cu}_2\text{ZnSnS}_4$ Thin Film Solar Cell with over 9% Efficiency. *Adv. Energy Mater.* 5 (2015) 1500682
- [4] C. Yan, K. Sun, J. Huang, S. Johnston, F. Liu, B. Puthen Veetil, K. Sun, A. Pu, F. Zhou, J. A. Stride, M. A. Green, and X. Hao. Beyond 11% Efficient Sulfide Kesterite $\text{Cu}_2\text{ZnxCd}_{1-x}\text{SnS}_4$ Solar Cell: Effects of Cadmium Alloying. *ACS Energy Lett.* 2 (2017) 930
- [5] Z.-Y. Xiao, Y.-F. Li, B. Yao, R. Deng, Z.-H. Ding, T. Wu, G. Yang, C.-R. Li, Z.-Y. Dong, L. Liu, L.-G. Zhang, H.-F. Zhao. Band gap engineering of $\text{Cu}_2\text{CdxZn}_{1-x}\text{SnS}_4$ alloy for photovoltaic application: a complementary experimental and first-principles study. *J. Appl. Phys.* 114 (2013) 183506
- [6]. Montoya De Los Santos, Maykel Courel, N.R. Mathews, X. Mathew. Study on the effect of annealing under pressure on the material properties of $\text{Cu}_2\text{ZnSn}(\text{S},\text{Se})_4$ thin films. *Materials Science in Semiconductor Processing* 68 (2017) 68
- [7] A.S. Ibraheem, Y. Al-Douri, U. Hashim, M.R. Ghezzar, A. Addou, W. K. Ahmed. Cadmium effect on optical properties of $\text{Cu}_2\text{Zn}_{1-x}\text{CdxSnS}_4$ quinary alloys nanostructures. *Solar Energy* 114 (2015) 39

- [8] A S Ibraheam, Y Al-Douri, S C B Gopinath and U Hashim. A novel quinary alloy ($\text{Cu}_2\text{Zn}_{1-x}\text{Cd}_x\text{SnS}_4$) nanostructured sensor for biomedical diagnosis. *Mater. Res. Express* 3 (2016) 085022
- [9] Q. Zhang, H. Deng, L. Chen, L. Yu, J. Tao, L. Sun, P. Yang, J. Chu. Cation substitution induced structural transition, band gap engineering and grain growth of $\text{Cu}_2\text{Cd}_x\text{Zn}_{1-x}\text{SnS}_4$ thin films. *Journal of Alloys and Compounds* 695 (2017) 482
- [10] L. Meng, B. Yao, Y. Li, Z. Ding, Z. Xiao, K. Liu, G. Wang. Significantly enhancing back contact adhesion and improving stability of $\text{Cu}_2(\text{Zn,Cd})\text{Sn}(\text{S,Se})_4$ solar cell by a rational carbon doping strategy. *Journal of Alloys and Compounds* 710 (2017) 403
- [11] J. Fu, Q. Tian, Z. Zhou, D. Kou, Y. Meng, W. Zhou, and S. Wu. Improving the Performance of Solution-Processed $\text{Cu}_2\text{ZnSn}(\text{S,Se})_4$ Photovoltaic Materials by Cd^{2+} Substitution. *Chem. Mater.* 28 (2016) 5821
- [12] A. S. Ibraheam, Y. Al-Douri, J. M. S. Al-Fhdawi, H. S. AL-Jumaili, K. D. Verma, U. Hashim, R. M. Ayub, A. Rahim Ruslinda, M. K. Md Arshad, A. H. Reshak, S. B. Abd Hamid. Structural, optical and electrical properties of $\text{Cu}_2\text{Zn}_{1-x}\text{Cd}_x\text{SnS}_4$ quinary alloys nanostructures deposited on porous silicon. *Microsystem Technologies* 22 (2016) 2893
- [13] A. S. Ibraheam, Y. Al-Douri, N. Z. Al-Hazeem, U. Hashim, D. Prakash, and K. D. Verma. Effect of Cadmium Concentration on Structural, Optical, and Electrical Properties of $\text{Cu}_2\text{Zn}_{1-x}\text{Cd}_x\text{SnS}_4$ Quinary Alloy Nanofibres, Synthesized by Electrospinning Technique. *Journal of Nanomaterials* 2016 (2016) 7314714
- [14] W. Wang, M. T. Winkler, O. Gunawan, T. Gokmen, T. K. Todorov, Yu Zhu, David B. Mitzi. Device Characteristics of CZTSSe Thin-Film Solar Cells with 12.6% Efficiency. *Adv. Energy Mater.* 4 (2014) 1301465
- [15] M. Pilvet, M. Kauk-Kuusik, M. Altosaar, M. Grossberg, M. Danilson, K. Timmo, A. Mere, V. Mikli. Compositionally tunable structure and optical properties of $\text{Cu}_{1.85}(\text{Cd}_x\text{Zn}_{1-x})_{1.1}\text{SnS}_{4.1}$ ($0 \leq x \leq 1$) monograin powders. *Thin Solid Films* 582 (2015) 180
- [1] T. Maeda, S. Nakamura, T. Wada. First-principles study on Cd doping in $\text{Cu}_2\text{ZnSnS}_4$ and $\text{Cu}_2\text{ZnSnSe}_4$. *Jpn. J. Appl. Phys.* 51 (2012) 365
- [2] Y. Zhang, X. Sun, P. Zhang, X. Yuan, F. Huang, and W. Zhang. Structural properties and quasiparticle band structures of Cu-based quaternary semiconductors for photovoltaic applications. *Journal of Applied Physics* 111 (2012) 063709
- [3] Q. Zhang, H. Deng, L. Chen, J. Tao, J. Yu, P. Yang, J. Chu. Effects of sulfurization temperature on the structural and optical properties of $\text{Cu}_2\text{CdSnS}_4$ thin films prepared by direct liquid method. *Materials Letters* 193 (2017) 206
- [4] M. Mourad Mabrook, *Exp. Theo. NANOTECHNOLOGY* 2 (2018) 103
- [5] S. Chen, A. Walsh, X.-G. Gong, S.-H. Wei. Classification of lattice defects in the kesterite $\text{Cu}_2\text{ZnSnS}_4$ and $\text{Cu}_2\text{ZnSnSe}_4$ earth-abundant solar cell absorbers, *Adv. Mater.* 25 (2013) 1522